Research Article
doi.org/10.1002/elsa.202100189

Chemistry Europe
European Chemical Societies Publishing

Received: 22 October 2021
Revised: 26 November 2021
Accepted: 14 January 2022

Ionic transport modeling for liquid electrolytes - Experimental evaluation by concentration gradients and limited currents

Maximilian Schalenbach | **Burkhard Hecker** | **Bernhard Schmid** | **Yasin Emre Durmus** | **Hermann Tempel** | **Hans Kungl** | **Rüdiger-A. Eichel**

Fundamental Electrochemistry (IEK-9), Forschungszentrum Jülich GmbH, Institute of Energy and Climate Research, Wilhelm-Johnen-Str. 1, Jülich 52425, Germany

Correspondence
Maximilian Schalenbach, Fundamental Electrochemistry (IEK-9), Institute of Energy and Climate Research, Forschungszentrum Jülich GmbH, Jülich, 52425 Germany.
Email: m.schalenbach@fz-juelich.de

Funding information
German Federal Ministry of Education and Research, Grant/Award Number: 03SF0589A

Abstract

A direct current in an electrochemical cell with a diluted liquid electrolyte leads to the displacement of ions within the solvent, while diffusion works against the resulting concentration differences. This study aims to experimentally evaluate a physicochemical ion transport model (source code provided) that describes current-driven concentration gradients in diluted electrolytes. Hereto, an aqueous 0.1 M $CuSO_4$ electrolyte between metallic copper electrodes serves as an experimental test system. Spatially resolved optical measurements are used to monitor the evolution of the ion concentration gradient in the electrolyte. Moreover, measured limited currents are related to computationally modeled concentration gradients. A constant parameterization of the diffusion coefficient, molar conductivity and ion transport number lead to a slight overestimation of the cathodic ion depletion and cell resistance, whereas a literature data based concentration dependent parameterization matches better to the measured data. The limited current is considered under a computational parameter variation and thereby related to the physicochemical impact of different electrolyte properties on the ion transport. This approach highlights the differences between purely diffusion limited currents and the limited current resulting from the combined electric field and diffusion driven ion motion. A qualitative schematic sketch of the physical mechanisms of the ion movement is presented to illustrate the current driven ion displacement in liquid electrolytes.

KEYWORDS
conductivity, differential equations, diffusion, diffusion-limited current, liquid electrolyte

1 | INTRODUCTION

The charge exchanged between the electrodes in electrochemical cells is carried by moving ions in the electrolyte. In the 19th century, Hittorf first observed current-driven concentration changes in the anodic and cathodic compartments during the electrolysis of aqueous electrolytes. From these experiments, he derived the ion transport number[1–3] that describes the contributions of different ions to the overall conductivity.[4] The concentration

Research Article
doi.org/10.1002/elsa.202100189
Chemistry Europe
European Chemical Societies Publishing

gradients that result from the electrochemical ion transport in binary diluted electrolytes were observed for example by spatially resolved nuclear magnetic resonance spectroscopy in Li-ion battery electrolytes.[5–7] Such concentration gradients limit electrochemical currents and increase cell resistances, for which a detailed knowledge about the ion transport is of great importance for electrochemical systems and applications that operate with liquid electrolytes.

The ions in the bulk of an equilibrated electrolyte solution are evenly distributed. In the electrostatic equilibrium (no current), potential differences between the electrodes are locally shielded at the electrode-electrolyte interfaces by potential drops over just a few molecular layers in the double layer,[8–11] in which ions with opposing charges are at least partly spatially separated.[12] In this equilibrium, the bulk electrolyte avoids (like every other conductor) electric fields in its inside. Electrochemical reactions at the electrodes lead to an electrodynamic state, where the ion transport is driven by the electric field (according to Ohms law) inside the electrolyte. In liquid diluted electrolytes, the migration caused by the electric field moves positively and negatively charged ions in opposing directions. The resulting displacement of ions in diluted liquid electrolytes is counteracted by diffusion, which works against concentration gradients.

In the 1970s, the current-driven concentration gradients in aqueous copper sulfate solutions were analytically calculated and compared to optical measurements.[13–15] Further models to calculate the evolution of current-driven concentration gradients[16–18] followed, which typically use a constant and concentration-independent parameterization of the molar conductivity, diffusion coefficients, and transfer numbers. However, the interactions between the ions (described by the Debye-Hückel theory[19,20]) lead to concentration dependence of these electrolyte parameters, which were thus far not included in the reported models.

This study reports on an experimental evaluation of a physical model for ion transport and the related spatiotemporal concentration gradients and limited currents. The presented physical model operates in a computational numerical framework that enables a concentration-dependent parametrization of electrolyte parameters. Moreover, varying boundary conditions such as current profiles can be fed into the numerical framework. An aqueous $CuSO_4$ electrolyte and copper electrodes are chosen as an exemplary model system, as the concentration dependence of the conductivity, mutual diffusion coefficients, and transfer coefficients of the $CuSO_4$ electrolyte are reported and as the copper ion concentration is optically observable by the solution color. Furthermore, the electrochemistry of cathodic copper deposition and anodic copper dissolution come with low overpotentials and high current efficiencies within the electrochemical window of water.[21–23] The ion transport is modeled for a constant and a concentration-dependent parameterization of the electrolyte parameters. The outcome of both parameterization approaches is compared to the experimental data. A computational parameter variation on the electrolyte properties is conducted, showing how the electrolyte parameters influence limited currents.

2 | METHODS

All measurements were conducted in a temperature-controlled lab with an operating temperature of $20 \pm 0.2°C$. The computational simulation was performed with a personal computer without advanced hardware specifications.

2.1 | Optical monitoring of concentration gradients

An in-house made glass cell with optical windows was used to optically monitor the spatiotemporal concentration of copper ions in an aqueous 0.1 M $CuSO_4$ electrolyte between an electro-dissolving copper anode and an electro-depositing copper cathode. Pictures through the optical windows of this glass cell were recorded with a digital industry camera (Basler ACE) in order to monitor the light adsorption of the electrolyte. The distance between the parallel aligned copper electrodes was 7.1 mm, while an Ag/AgCl reference electrode was connected to the feed of the cell. The glass cell was operated with a constant current of 1.5 mA/cm^2 and an AC modulation at 5 kHz[1] (with an amplitude of 2% of the applied direct current) to measure the resistance. Further details on the experimental setup are described in the supporting information (SI) to this article provided online.

Figure 1a shows a picture that was taken by the camera at the end of the measurement procedure,which displays a distinct color gradient between the anode (bottom) and cathode (top). The white balance of this picture was conducted using a picture of the optical window without electrolyte (see SI for details). The detailed picture analysis and the corresponding computer code are supplied in the SI. In brief, the ratio of the blue to the red component of the RGB (red-green-blue) pixels was determined. Figure 1b shows the calibration curve of the blue over the red com-

[1] As the software of the potentiostat does not supply a method with a steady galvanostatic frequency, a frequency scan with 1000 steps between 5 and 5.1 kHz was used to measure at an approximately constant frequency over time.

Research Article
doi.org/10.1002/elsa.202100189
Chemistry Europe
European Chemical Societies Publishing

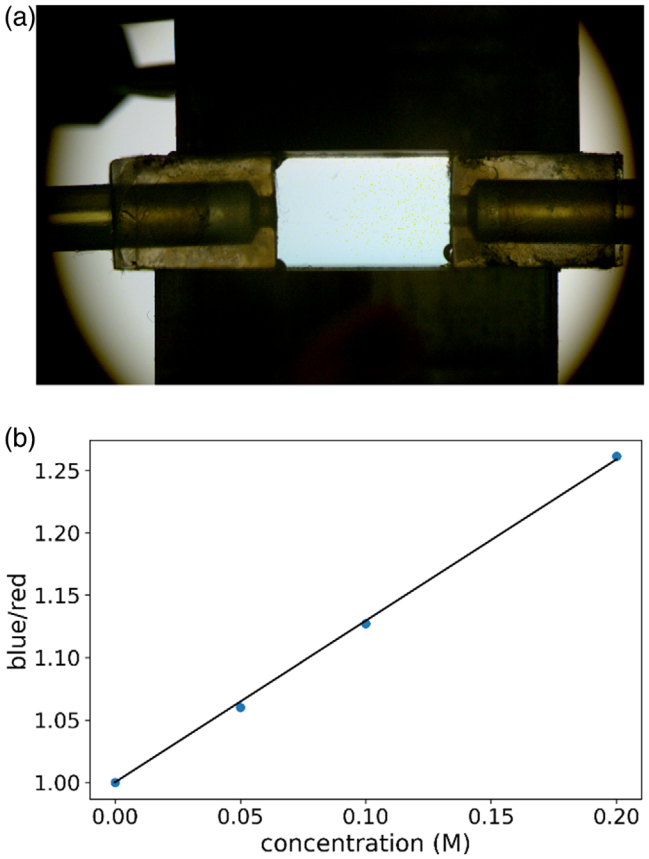

FIGURE 1 (a) A picture taken by the digital camera in the apparatus at the end of a measurement. The color gradient from light blue at the top (cathode) to a deeper blue at the bottom (anode) shows the concentration gradient in the cell. (b) Calibration curve to relate the solution color to the copper ion concentration. The ratio of the blue component to the red component of the red-green-blue (RGB) values of the camera pictures is shown as a function of the concentration of four different equilibrated electrolytes. Blue scatter: measured values. Solid black line: linear fit

ponent against different molar solutions. A linear fit was conducted to these data, from which the spatially resolved solution color is related to the concentration.

2.2 | Experiments to determine limited currents

A cell with a distance of 480 μm between the electrodes was used to examine a steady state of a limited current under potentiostatic conditions. Hereto, a potential of 0.3 V was applied with 5 mV perturbation at 5 kHz to simultaneously measure the current and the resistance of the cell as a function of time. With this cell an optical measurement of the concentration cannot be conducted, however, due to the small distance between the electrodes a steady state is reached faster than that of the glass cell. The two polished copper electrodes were pressed onto one another and separated by a stamped fluoroelastomer flat sealing with an inner diameter of 14 mm and a thickness of 480 μm (Reichelt Chemietechnik, Germany). Further details on the setup are provided in the SI.

2.3 | Physical simulation

The physical simulation used to describe the current-driven spatiotemporal ion concentration in the electrolyte is based on a system of differential equations that are derived from the continuity equation with diffusion (Fick's law) and electric field (Ohm's law) driven ion motion. Local spatial electroneutrality is presumed, as any local difference of charge leads to strong electric fields that are instantaneously balanced by conduction-driven ion movement. In the case of the binary $CuSO_4$ electrolyte used in this study, the local electroneutrality means that the spatiotemporal concentration of the cation equals that of the anions. Convective forces such as electrolyte flows,[24,25] stirring,[26] ascending bubbles,[27,28] or local density differences that lead to gravitational shear forces[29] are not considered in the model. The distance d between the electrodes resembled that from the experiment (7.1 mm for the glass cell and 0.48 mm for the other cell). The time increment Δt was chosen to a fraction of 10^{-5} of the total time considered in the simulation, while the spatial resolution Δx was one hundreds of d.

Previous works reported similar approaches for ionic transport models,[16–18] nevertheless, a detailed step-by-step derivation of the differential equations is discussed in the SI. The developed simulation solely represents the transport mechanisms in the bulk electrolyte and is current-based, so that the electrode potential with its numerous effects on the kinetics, thermodynamics (Nernst equation), and double-layer is not involved in the calculations. The model input consists of cell parameters (current density, initial electrolyte concentration, and electrode distance) and literature data on concentration-dependent conductivity, mutual diffusion coefficients, and transfer numbers. The boundary conditions of a given constant or time-dependent current profile can be considered in the model to resemble the experimental approaches presented above. The source code for the implementation in the programming language Python is provided in the SI.

2.4 | Modeled cell resistance

The concentration gradient in the cell leads to locally different conductivities. Based on the modeled concentration gradients the overall cell resistance can be calculated and compared to the data from impedance measurements. The results of the calculated spatiotemporal concentration are

Research Article
doi.org/10.1002/elsa.202100189
Chemistry Europe
European Chemical Societies Publishing

summarized in a matrix $\overline{\overline{c}}$, where one dimension represents the time and the other the spatial position. Based on this calculated concentration matrix, a conductivity matrix $\overline{\overline{\kappa}}$ of every discrete part in the time-space can be calculated by

$$\overline{\overline{\kappa}} = \overline{\overline{c}} \circ \overline{\overline{\Lambda}}\left(\overline{\overline{c}}\right), \tag{1}$$

where $\overline{\overline{\Lambda}}(\overline{\overline{c}})$ has the same matrix dimensions as $\overline{\overline{c}}$ and provides a value for the molar conductivity for every matrix element of the concentration. The Hadamard product (element-wise matrix multiplication) connects the concentration matrix $\overline{\overline{c}}$ and the molar conductivity matrix $\overline{\overline{\Lambda}}(\overline{\overline{c}})$, so that the conductivity matrix $\overline{\overline{\kappa}}$ describes the same spatiotemporal framework as the other matrices. Including the geometry of the spatial increment of the electrode area A (set to 1 cm^2) and the spatial increment Δx leads to the conductance matrix $\overline{\overline{G}}$:

$$\overline{\overline{G}} = \frac{A}{\Delta x}\overline{\overline{\kappa}} \tag{2}$$

By inverting every single element of the conductance matrix $\overline{\overline{G}}$ the resistance matrix $\overline{\overline{R}}$ can be calculated. From this resistance matrix the total resistance of the electrolyte as a function of time (vector $\bar{R}$) can be calculated as the sum over the spatial component.

$$\overline{R_t} = \sum_x \overline{\overline{R}}_{x,t} \tag{3}$$

2.5 | Modeling limited currents

Limited currents are modeled by starting the simulation with a higher current than the supposed limited current. When the electrolyte concentration at the cathode depletes, the current is incrementally adjusted, so that the cathodic ion concentration remains negligible. In detail, when the cathodic concentration drops below 1/15 of the initial concentration the current is slightly increased while it is increased when the concentration is above 1/12. Using these boundary conditions, the simulation runs into a steady-state with a limited current and a constant concentration gradient.

2.6 | Parametrization

The molar conductivities, mutual diffusion coefficients, and transport numbers of copper sulfate as a function of the ionic strength are reported in the literature[30–34] and

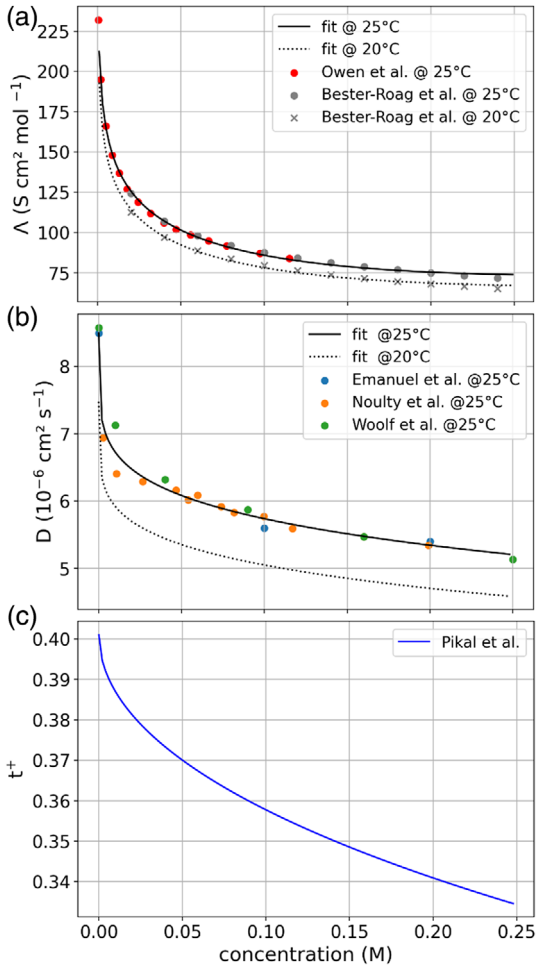

FIGURE 2 Concentration dependence of the electrolyte parameters. Black solid lines: Fits by Equations (4) and (5). Scatter: literature data. (a) Molar conductivity. (b) Mutual diffusion coefficient. (c) The equation of the transfer coefficient for copper ions in copper sulfate solution reported by Pikal et al.,[36] is based on the transfer coefficients reported by various authors

graphed in Figure 2. The data on the molar conductivity were fitted by a power law dependency with the parameters P_1, P_2 and P_3:

$$\Lambda\ (c) = P_1\ - P_2 c^{0.005} + P_3 c \tag{4}$$

The literature data for the mutual diffusion coefficient was fitted with a similar equation:

$$D\,(c) = P_1\ - P_2\ c^{P_3} \tag{5}$$

Both equations do not represent a physical meaning, they are used to resemble a simple mathematical description of the reported literature data. The diffusion coefficients of both ions are different,[35] whereas they can only diffuse pairwise in order to maintain the local electroneutrality of the electrolyte. Thus, their combined value in the

Research Article
doi.org/10.1002/elsa.202100189
Chemistry Europe
European Chemical Societies Publishing

form of the mutual diffusion coefficient and not their individual values are decisive for the overall diffusion.

Figure 2a,b graph fits for 20 and 25°C. In the case of the molar conductivity, the two dimensional parameter room that describes the effect of concentration and temperature on the molar conductivity was reported by Bešter-Rogač et al.,[33] showing that the conductivity at 20°C is approximately 91% of that at 25°C. In the case of the mutual diffusion coefficient of copper sulfate such a detailed parameterization is not reported. However, the effect of temperature on diffusion coefficient was reported by Moats et al.[37] to

$$D = D_0\, e^{-E_D/RT}, \tag{6}$$

with $D_0 = 0.0112\ \mathrm{cm^2/s}$, $E_D = 19.2\ \mathrm{kJ/mol}$ and the gas constant R. Using this equation, the mutual diffusion coefficient at 20°C is determined to 88% of that at 25°C. Figure 2c shows the transfer number t^+ for the copper ions in copper sulfate solutions reported by Pikal et al.,[36] which reported a function for the concentration dependence that is based on a detailed comparison of the results of different authors:

$$t^+ = 0.401 - 0.1426\ \sqrt{c} + 0.0186\ c \tag{7}$$

The authors of this study also reported that temperature between 4 and 25°C has little impact on the transfer number, for which the temperature dependence is neglected in the presented model. The dissolution of copper sulfate acidifies the solution so that additional protons are introduced into the electrolyte. A detailed discussion on the influence of the pH effect on ion transport is discussed in the SI, showing that the pH has a minor impact on the measured data, and thus it is included in the transport model.

3 | RESULTS AND DISCUSSION

All measurements were conducted with polished copper electrodes and a 0.1 M $CuSO_4$ electrolyte at a temperature of 20°C. Two different parameterizations of the model are considered in the following: (i) A constant parameterization, where the molar conductivity, mutual diffusion coefficient, and transfer numbers refer to the values of the fits in Figure 2a,b at a concentration of 0.1 M (which equals the starting concentration of the expeirments). (ii) A concentration dependent parameterization, where these electrolyte parameters are calculated as a function of the concentration by the fits that are graphed in Figure 2 for each spatial element in the model.

The model and measurements are compared for two different conditions: 1) A constant current is applied to the glass cell with an electrode distance of 7.1 mm (see description above), in order to optically monitor the evolution of the concentration gradient between the electrodes. These experimental data is directly compared to the modeled data. 2) A constant voltage is applied to the cell with the 480 μm electrode distance in order to reach the limited current. The current profile of the experiment is fed into the model and the cathodic copper depletion predicted by the model is related to the measured limited current. At the limited current the system reaches a steady state with a time independent concentration profile.

After evaluating the validity of the modeled data, a parameter analysis discusses the effect of the different electrolyte parameters on the limited current. Based on these results, the physical mechanisms of ion transport are considered in detail. A schematic illustration for ion transport is presented, which provides a qualitative understanding of how the differential equations of the numerical model work and how the physical transport mechanisms contribute to the evolution of concentration gradients.

3.1 | Experimental evaluation at constant current

In the following, a constant current density of 1.5 $\mathrm{mA/cm^2}$ is applied to the glass cell (7.1 mm electrode distance). Three data sources are compared, including the measured electrochemical data (impedance, cell voltage and cathodic overpotential), the optically measured spatiotemporal concentration in the bulk solution of the glass cell and the calculated model outcome (resistance and spatiotemporal concentration in the electrolyte). The current density of 1.5 $\mathrm{mA/cm^2}$ leads to slowly forming concentration gradient and exceeds the limited current of this configuration so that a cathodic copper ion depletion is expected. The data of one measurement is discussed here, while the data of four repetitions are shown in the SI in order to ensure the reproducibility.

Figure 3a shows the measured time evolution of the cell voltage and the cathodic overvoltage (absolute voltage between the cathode and the reference electrode) that are measured with the above described experimental setup. The current was applied at $t = 0$ s, while cell voltage and cathodic overvoltage slightly increase over time. Beginning at 1900 s the voltage increase is accelerated until at about 2000 s the cathodic overvoltage and the cell voltage both increased by approximately 0.5 V compared to their initial values. At the cathode, the copper ions are deposited while the sulfate anions are attracted by the electric field towards the anode. Consequently, the concentration of dissolved ions at the anode increases while it decreases at the cathode. As soon as the concentration of copper ions at the

Research Article
doi.org/10.1002/elsa.202100189

Chemistry Europe
European Chemical Societies Publishing

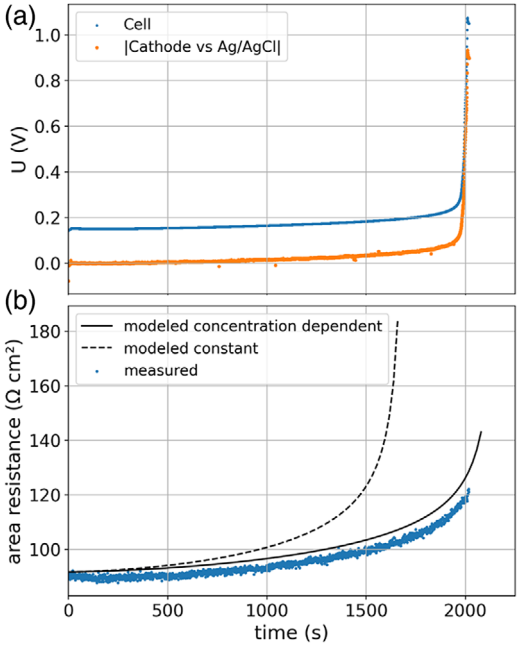

FIGURE 3 Electrochemical measurements of the 0.1 M $CuSO_4$ electrolyte in the glass cell under a galvanostatic current density of 1.5 mA/cm^2 as a function of time. (a) Cell voltage and the absolute voltage between the cathode and the Ag/AgCl reference electrode. At about 2000 seconds the cathodic overpotential drastically increases due to the transition from cathodic copper deposition to the hydrogen evolution reaction. (b) Modeled and measured area resistances. The area resistance increases over time as the ion concentration near the cathode is thinning out

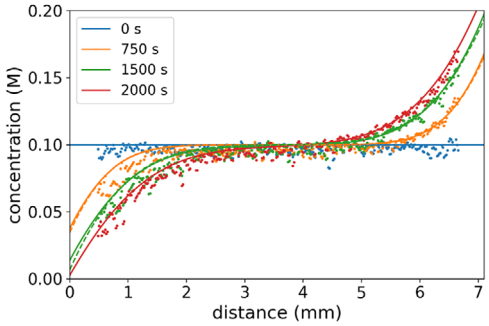

FIGURE 4 Measured (scatter) and modeled (lines) spatial electrolyte concentration profiles between the electrodes at a current density of 1.5 mA/cm^2 with a 0.1 M electrolyte. Solid lines: Simulation with concentration-dependent coefficient diffusion and molar conductivity. Dashed lines: Simulation with constant parameters (for 2000 s no data as the limited current was already exceeded after 1970 s). The cathode is at 0 mm, while the anode is at 7.1 mm. The experimental data in this figure have been recorded simultaneously to those graphed in Figure 3

cathode is not sufficient to maintain the copper deposition current, the cathodic overpotential increases. To maintain the applied galvanostatic current under copper ion starvation at the cathode, the hydrogen evolution reaction[38,39] ($2H_2O \rightarrow 2H_2 + 2OH^-$) partly replaces the copper deposition. An increase of the cathodic overpotential results, as the standard potential of the Redox-couple Cu/Cu^{2+} of 0.34 V drops to that of the hydrogen evolution (0 V at $pH = 0$). The produced hydroxide ions by the hydrogen evolution reaction locally reduce the pH and thereby further decrease the reversible potential, for which a drastic increase of the overpotential is observed.

Figure 3b shows the modeled and measured area resistance of the cell, which was measured by a 5 kHz perturbation on the current via impedance (see experimental section for details). It steadily increases from approximately 90 to 120 Ohms/cm^2 over the time measured. At the cathode, the ion depletion leads to an increasing local resistivity, while it decreases at the anode due to ion accumulation. The overall resistance as a serial connection of all local resistances increases. If the concentration in the bulk electrolyte close to the electrode is negligible, the resistivity would increase to infinity. However, at the time that the cathodic overpotential increases and the cathodic copper deposition is replaced by the hydrogen evolution, hydroxide ions penetrate into the electrolyte. Therefore, a non-conductive gap of pure water directly at the cathode does not appear.

Using the constant parameterization, the modeled area resistance increases more drastically than that of the experiment. The concentration-dependent parameterization leads to slightly smaller values than those measured. The constant parameterization led to a negligible copper ion concentration at the anode at about 1660 s, whereas this point is reached with concentration-dependent parameterization at approximately 2080 s. The modeled resistances with the concentration-dependent parameterization are approximately 4% smaller than the measured one over the entire time scale considered, which is within the expectable measurement precision.

Figure 4 shows the optically measured and computationally simulated spatiotemporal concentrations of copper ions in the electrolyte between the electrodes. The experimental data with distances less than 500 μm to the electrodes was removed, as these were affected by measurement errors (see detailed experimental description in the SI). The modeled and measured spatiotemporal concentration are shown for four different times, namely 0, 750, 1500 and 2000 s after the current has been switched on. The measured data is affected scattering in the range of 0.01 M which is attributable to the camera noise. Within the estimated maximum spatial error of 500 μm of the optical measurement (see SI), modeled and measured data reasonably agree.

Research Article
doi.org/10.1002/elsa.202100189
Chemistry Europe
European Chemical Societies Publishing

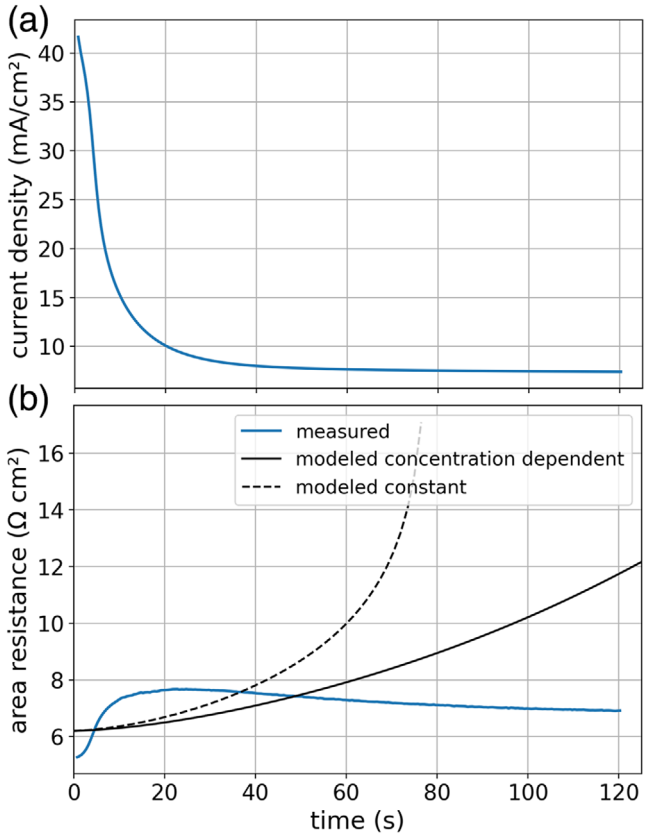

FIGURE 5 Electrochemical measurements on the cell with the electrode distance of 480 μm and a constant cell voltage of 0.3 V as a function of time. (a) Current density as a function of time. A limited current density of 7.5 mA/cm^2 results. (b) Measured and modeled area resistances

3.2 | Experimental evaluation at constant voltage

In the following, the electrochemical response of the Cu-$CuSO_4$ system is considered under a constant voltage of 0.3 V. This voltage is large enough to supply the overpotentials for the copper deposition and dissolution but from a thermodynamic perspective, it is too small to lead to cathodic hydrogen evolution. Thus, a steady-state with a constant concentration gradient at the limited current is targeted. The cell with an electrode distance of 480 μm is used in the following, which has the following advantages in comparison to the glass cell with 7.1 mm electrode distance: (i) The time to reach a steady-state in the form of a limited current is smaller. (ii) Higher current densities are possible. (iii) The impact of the changing surface morphology of the electrodes during the short measurement time on the limited current density is negligible. However, optical measurements of the concentration gradients are not possible.

Figure 5 shows the current as a function of time for the applied voltage of 0.3 V. Starting with a current of

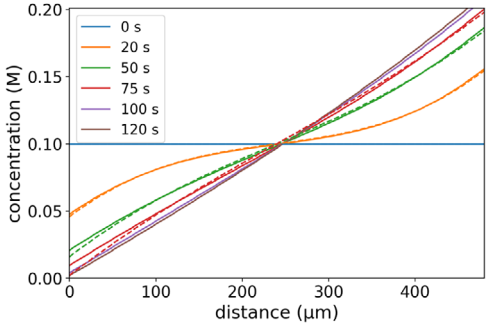

FIGURE 6 Modeled time evolution of the concentration gradient for the $CuSO_4$ electrolyte in the cell with the 480 μm electrode distance (referring to the data graphed in Figure 5). Solid lines: With a concentration-dependent parameterization. Dashed lines: With a constant set of parameters, where the cathodic ion depletion is reached after approximately 77 s

42 mA/cm^2 the current decays after 90 s to an approximately constant value of approximately 7.5 mA/cm^2. The measured area resistance rapidly increases within 20 s from approximately 5.5 to 7.7 Ω cm^2, from which it goes back to approximately 7 Ω cm^2. The modeled area resistance with the concentration dependent parameterization starts at approximately the same value; however, it slowly increases over time to approximately 8.5 Ω cm^2 at the end of the measurement. The modeled values with the constant parameterization significantly exceeded the measured area resistance.

The measurement with the 7.1 mm electrode distance in Figure 3 showed a fine agreement of modeled and measured resistances, as the electrolyte resistance dominated and as the electrode processes had a marginal contribution to the overall resistance. With the more than tenfold smaller electrode distance, the resistances of electrolyte and the electrode processes become comparable. The anodic copper electrode may partly passivate during the high current densities and copper oxide may increase the resistance at the metal-electrolyte interface, which may explain the rapid increase of the cell resistance in the first 10 s of the experiment. However, to this point, the detailed physicochemical mechanisms that lead to the deviations between model and experiment are not clear and require further investigations.

Figure 6 shows the modeled spatiotemporal concentration in the electrolyte, using the current profile shown in Figure 5a as input. With the constant parameterization, the cathodic ion depletion is reached after approximately 77 s, so that the current cannot be maintained anymore. With the concentration dependent parameterization, the concentration profile just slightly changes after 100 s, which means that a steady state is reached, in which the cathodic copper concentration is low (0.01 M) but not

Research Article
doi.org/10.1002/elsa.202100189
Chemistry Europe
European Chemical Societies Publishing

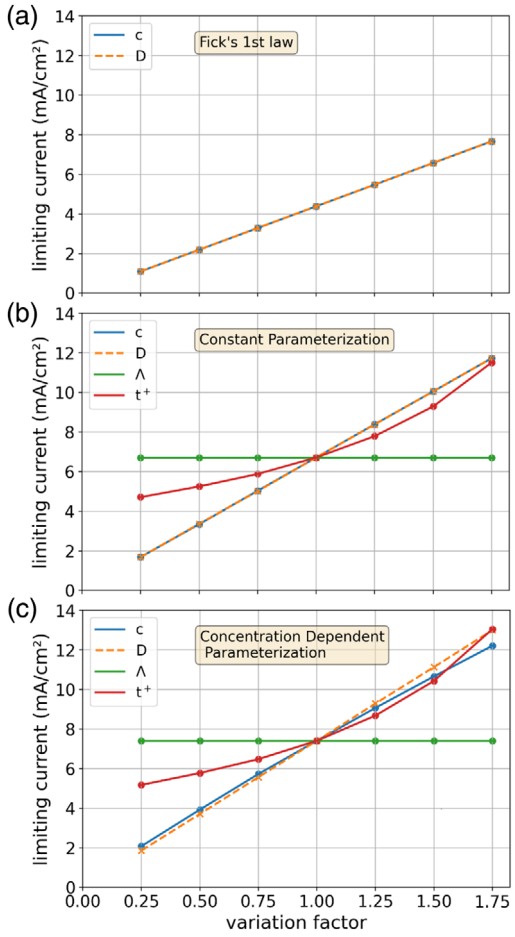

FIGURE 7 Modeled limited currents under a variation of the electrolyte concentration c, the diffusion coefficient D, the molar conductivity Λ and the transfer coefficient t^+. The variation factor displayed on the x-axis is multiplied by one of these parameters, while the others remain with their original values. (a) Calculation of the limited current by diffusion on the basis of Fick's first law (Equation (8)). (b) Modeled limited currents with a constant parametrization. (c) Modeled limited currents with the concentration-dependent parameterization

negligible. Accordingly, the modeled case with the concentration dependent parameterization resembles the experimental data with a steady state of the limited current.

3.3 | Computational electrolyte parameter variation

In the following, the impact of the electrolyte parameterization on the model outcome is examined for the following purposes: (i) To show how the uncertainty of measured parameters influences the results. (ii) To elucidate the effect of a parameter variation on the physicochemical transport mechanisms. Figure 7 shows the related results, where the x-axis displays the factor that is multiplied to the graphed electrolyte parameter while the other electrolyte parameters where unchanged. The non-changed values correspond to the values at 25°C that are graphed in Figure 2, while a distance between the electrodes of 480 μm is considered (similar to the previous experiment). Figure 7a shows the limited current calculated with Fick's first law, whereas Figure 7b,c shows the limited currents calculated with the model for the electric field and diffusion driven ion transport, using the procedure described in the 'methods sections'.

The results in Figure 7a for Fick's first law show the contributions of diffusion to the ion transport, excluding electric field driven contributions. In this non-electrochemical scenario the copper and sulfate ions are both taken away from one boundary (resembling the cathode), while the same amount is placed at the other boundary (resembling the anode). A constant concentration gradient results, while the concentration at one boundary is negligible. The limited current j_{lim} is calculated with Faradays law on the basis of the molar fluxes described by Fick's first law

$$j_{\text{lim}} = D\frac{\Delta c}{d}\,2F, \tag{8}$$

where Δc denotes the concentration difference between the anode and cathode, d the distance between the electrodes, and F the Faraday constant. For example, for an electrolyte concentration of 0.1 M, the concentration difference with a constant gradient is $\Delta c = 0.2$ M for a negligible ion concentration at one boundary. As the limited current in the equation is proportional to the concentration difference and the diffusion coefficient, the variation of both parameters has the same impact on the results.

For the constant parameterization graphed in Figure 7b, a variation of the diffusion coefficient and the concentration both influence the modeled results in the same manner as in Figure 7a. A variation of the molar conductivity does not affect the limited current. Towards larger values of the transfer coefficient t^+, the limited current increases as the copper ions carry more of the current and as the sulfate ions are less conducted towards the anode. With the concentration dependent parameterization graphed in Figure 7C, the mutual diffusion coefficient and transfer coefficient locally increase at the reduced cathodic concentrations (see Figure 2) which results in higher limited currents.

Using a variation factor of unity, the limited current is 4.4, 6.7, and 7.4 mA/cm^2 for the different scenarios graphed in Figures 7a–c. In the case of Figure 7a (results by Fick's first law), the limited current can be interpreted as a diffusion limited current, meaning that the diffusion carries the entire molar flux across the electrolyte. Such diffusion limited currents appear in real electrochemical system for example by the conversion of non-charged species such as

Research Article
doi.org/10.1002/elsa.202100189
Chemistry Europe
European Chemical Societies Publishing

the oxygen reduction, where a reactant depletion results in a diffusion limited current.[40–42] In this case, however, the reactant is not involved in the ion transport. The results in Figure 7b include the electric field driven contributions, so that the limited current is larger than the diffusion limited current. Thus, in this case, the limited current of the electrochemical ion transport by electric field and diffusion (as described by the model) is not to be confused with the diffusion limited current that is described by Fick's first law.

3.4 | Schematic model representation

To understand the evolution of the concentration gradients in more detail, Figure 8 shows a schematic sketch of the mechanism of the ion migration in the electrolyte. In this schematic sketch, four electrolyte compartments are illustrated, which resemble a reduced of amount the spatial elements of the numerical simulation. The electrodes resemble the boundary conditions of the differential equations, where the ions are deposited or introduced into the electrolyte. The molar flux of the ions between compartments are indicated by arrows. The current between each compartment must be equal (with reference to the continuity equation), meaning that the length of the error divided by the transported charge must be equal for every transfer between the compartments. The amount of copper sulfate in the electrolyte compartments is illustrated as bars (with reference to the electroneutrality in the solution, every compartment must have the same amount of copper and sulfate ions). Four different cases are sketched:

A. In the case of equilibrated solutions without any applied current, the same amount of ions is diffusing from the left to the right and vice versa, which results in no net ion movement. By applying a current, the state of equilibrium is left and a current-driven dynamic rearrangement of the ions in the solution starts. The entire current between the cathode and first compartment is carried by the deposited copper ions, as sulfate ions are not electrochemically converted. Analogously, the current between the anode and the fourth compartment is carried by the dissolving copper ions. The current between the electrolyte compartments is shared between sulfate ions and copper ions, while the proportion of the sulfate ions is larger due to their higher transfer number. In the beginning, diffusion plays a minor role as the concentration gradient is flat. Due to the different boundary conditions at the electrodes, the electrolyte starts to thin out at the cathode and concentrate at the anode.
B. A distinct concentration gradient evolves from the different mole fluxes between the compartments and diffusion influences the molar fluxes between the compartments. In the first compartment, the ion concentration is significantly lower than that in the second compartment, so copper and sulfate ions are diffusing along the concentration gradient. Thus,

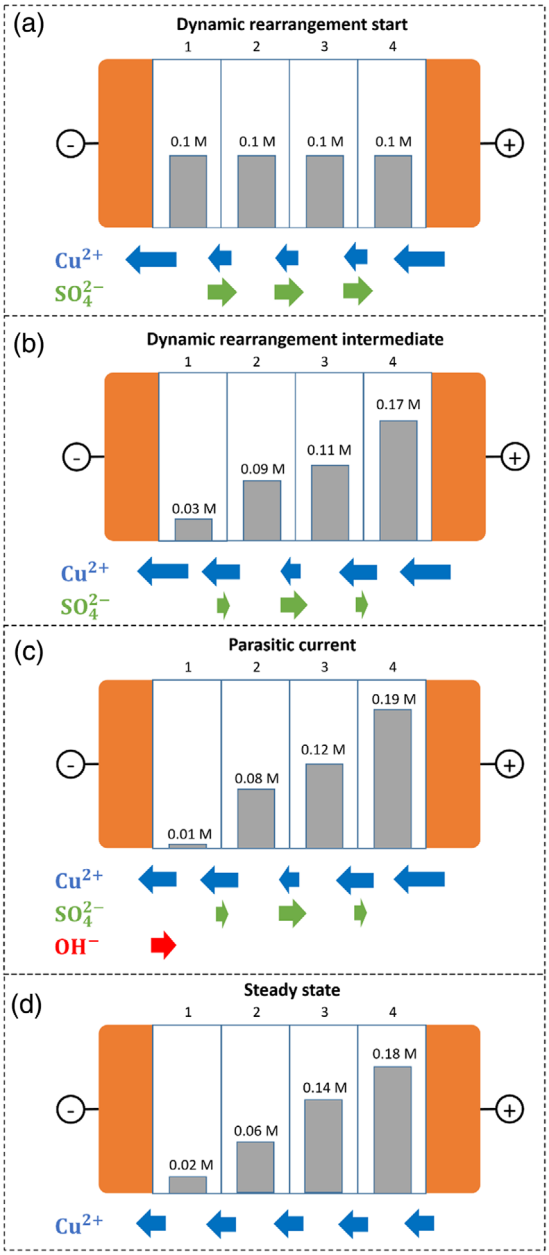

FIGURE 8 Schematic sketch of the ion movement in the electrolyte displayed for four different electrolyte compartments (1–4) between the cathode and anode. The arrows represent the molar fluxes between the compartments of the different ion types. Four different cases are considered: (a) Dynamic rearrangement starting with an equilibrated solution. (b) Intermediate state of the dynamic rearrangement, where a distinct concentration gradient is evolved but the concentration still changes over time. (c) Parasitic currents due to electrolyte decomposition. (d) Steady-state with a constant concentration gradient

Research Article
doi.org/10.1002/elsa.202100189

the electric field-driven migration of the sulfate ions from the first to the second compartment is damped by diffusion, whereas diffusion supports the current of the copper ions in the other direction. A similar concentration gradient appears between the third and fourth compartments. Between the second and third compartments, the concentration gradient is smaller and thus the current between both compartments is more equally shared between copper and sulfate ions. In the fourth compartment, the electrolyte is concentrated, as sulfate ions are attracted to the anode, and at its interface with the anode copper ions are steadily introduced. Depending on the applied current, this case can result in the two different scenarios that are discussed in the following.

C. When the applied current is higher than the limited current, it cannot be carried by the copper ions anymore as their concentration in the first department becomes too low. In this case, the electrolyte is decomposed, leading to a parasitic current of hydroxide ions that comes from the cathodic water splitting.[43] The new ion species introduced into the electrolyte changes reduce the solubility of copper sulfate, leading to different electrolyte compositions and behavior.
D. A current that is smaller than the limited current means that in the first compartment enough copper ions are present to maintain the copper ion deposition. After the dynamic rearrangement, a steady-state with a constant concentration gradient is reached, where the amount of sulfate ions diffusion along the concentration gradient is equal to the amount that is carried by the current. Thus, the net molar flux of sulfate ions between the compartments is negligible. In this case, diffusion and electric field drive the copper motion from the anode to the cathode.

3.5 | Simulation applicability to other systems

This study focused on a binary electrolyte, where one cation type and one anion type are dissolved in a polar solvent. The solvation of the ions allows them to travel independently through the electrolyte as long as the macroscopic electroneutrality is maintained. In the discussed case the cation was involved in the reactions while the anion was inert. The boundary conditions of the numerically solved differential equations define whether the different ion types are involved in the electrode reactions or whether they are inert. Accordingly, cases in which anions are involved in the reactions can be easily modeled by changing the boundary conditions.

The concentration gradients described by the model cannot appear in polymer membranes, where a moveable ion type is attracted by the Columbia force to immobile ions that are chemically bonded to the polymer matrix.[44,45] In such a system, only microscopic perturbances of the ion positions are possible, whereas a macroscopic ion displacement of the moveable ion types would directly result in a violation of the electroneutrality and would be instantaneously balanced by the conduction of the mobile ion type itself. Another similar case with a rigid matrix of counter-ions is represented by solid-state conductors such as the solid proton or oxygen ion conductors.[46,47]

4 | CONCLUSIONS

In this study, the evolution of concentration gradients in an aqueous $CuSO_4$ electrolyte between two copper electrodes under an electrochemical current is computationally modeled and optically measured. Moreover, modeled and measured limited currents due to cathodic ion depletion are compared. With a concentration-dependent parameterization the local changes of molar conductivity, mutual diffusion coefficient, and transfer number t^+ concentration gradient in the solution is included, leading to precise modeling of measured concentration gradients and limited currents. Under a variation of the electrolyte parameters in the ion transport model, the physicochemical properties that affect the ion transport and related limited currents are highlighted. Therewith, differences between diffusion-limited currents (described by Fick's first law) and the limited current by the combined electric field and diffusion-driven ion transport are discussed. To illustrate the physics behind the differential equations of ion transport, a qualitative scheme is discussed to show the causes of the ion displacement in the electrolyte. In the presented framework, the simulation has proven its reliability for two different scenarios, galvanostatic and potentiostatic conditions (operated at more than tenfold different current densities and electrode distances), precisely predicting the cathodic ion depletion that leads to parasitic reactions or limited currents.

ACKNOWLEDGEMENT

This work was supported by the German Federal Ministry of Education and Research (BMBF) within Project iNEW (03SF0589A).

Open access funding enabled and organized by Projekt DEAL.

CONFLICT OF INTEREST

The authors declare no conflict of interest.

Research Article
doi.org/10.1002/elsa.202100189
Chemistry Europe
European Chemical Societies Publishing

DATA AVAILABILITY STATEMENT

The data that support the findings of this study are available on request from the corresponding author. The data are not publicly available due to privacy or ethical restrictions.

REFERENCES

1. R. Guidelli, R. G. Compton, J. M. Feliu, E. Gileadi, *IUPAC Tech. Rep.* **2014**, *86*, 245.
2. M. B. Kristensen, A. Bentien, M. Tedesco, J. Catalano, *J. Colloid Interface Sci.* **2017**, *504*, 800.
3. M. Z. A. Munshi, B. B. Owens, S. Nguyen, *Polym. J.* **1988**, *20*, 587.
4. C. H. Hamann, A. Hamnett, W. Vielstich, *Electrochemistry*, 2nd ed. Wiley-VCH, Weinheim **2007**.
5. A. K. Sethurajan, S. A. Krachkovskiy, I. C. Halalay, G. R. Goward, B. Protas, *J. Phys. Chem. B* **2015**, *119*, 12238.
6. M. Klett, M. Giesecke, A. Nyman, F. Hallberg, R. W. Lindström, G. Lindbergh, I. Furó, *J. Am. Chem. Soc.* **2012**, *134*, 14654.
7. S. A. Krachkovskiy, A. D. Pauric, I. C. Halalay, G. R. Goward, *J. Phys. Chem. Lett.* **2013**, *4*, 3940.
8. B. B. Damaskin, O. A. Petrii, *J. Solid State Electrochem.* **2011**, *15*, 1317.
9. J. Huang, Y. Chen, *Curr. Opin. Electrochem.* **2019**, *14*, A4.
10. W. Schmickler, D. Henderson, *Prog. Surf. Sci.* **1986**, *22*, 323.
11. D. J. Bonthuis, S. Gekle, R. R. Netz, *Phys. Rev. Lett.* **2011**, *107*, 166102.
12. M. Schalenbach, Y. E. Durmus, H. Tempel, H. Kungl, R.-A. Eichel, *Phys. Chem. Chem. Phys.* **2021**, *23*, 21097.
13. Y. Awakura, Y. Kondo, *J. Electrochem. Soc.* **1976**, *123*, 1184.
14. A. Tvarusko, L. S. Watkins, *J. Electrochem. Soc.* **1971**, *118*, 248.
15. Y. Awakura, M. Okada, Y. Kondo, *J. Electrochem. Soc.* **1977**, *124*, 1050.
16. M. Van Soestbergen, P. M. Biesheuvel, M. Z. Bazant, *Phys. Rev. E Stat. Nonlinear Soft Matter Phys.* **2010**, *81*, 021503.
17. A. G. Zelinsky, B. Y. Pirogov, *Electrochim. Acta* **2009**, *54*, 6707.
18. D. Danilov, P. H. L. Notten, *Electrochim. Acta* **2008**, *53*, 5569.
19. M. Çetin, *Phys. Rev. E* **1997**, *55*, 2814.
20. A. Ferguson, I. Vogel, *Trans. Faraday Soc.* **1927**, *23*, 404.
21. J. Reid, *Jap. J. Appl. Phys.* **2001**, *40*, 2650.
22. D. Grujicic, B. Pesic, *Electrochim. Acta* **2002**, *47*, 2901.
23. N. Ibl, *Electrochim. Acta* **1977**, *22*, 465.
24. L. Dabrowski, T. Paczkowski, *Elektrokhimiya* **2005**, *41*, 102.
25. W. B. Gu, C. Y. Wang, J. W. Weidner, R. G. Jungst, G. Nagasubramanian, *J. Electrochem. Soc.* **2000**, *147*, 427.
26. S. Martens, L. Asen, G. Ercolano, F. Dionigi, C. Zalitis, A. Hawkins, A. Martinez Bonastre, L. Seidl, A. C. Knoll, J. Sharman, P. Strasser, D. Jones, O. Schneider, *J. Power Sources* **2018**, *392*, 274.
27. P. Boissonneau, P. Byrne, *J. Appl. Electrochem.* **2000**, *30*, 767.
28. D. Baczyzmalski, F. Karnbach, X. Yang, G. Mutschke, M. Uhlemann, K. Eckert, C. Cierpka, *J. Electrochem. Soc.* **2016**, *163*, E248.
29. G. W. Murphy, *J. Electrochem. Soc.* **1950**, *97*, 405.
30. A. F. W. Cole, A. R. Gordon, *J. Phys. Chem.* **1936**, *40*, 733.
31. L. A. Woolf, A. W. Hoveling, *J. Phys. Chem.* **1970**, *74*, 2406.
32. R. A. Noulty, D. G. Leaist, *J. Solution Chem.* **1987**, *16*, 813.
33. M. Bešter-Rogač, *J. Chem. Eng. Data.* **2008**, *53*, 1355.
34. B. B. Owen, R. W. Gurry, *J. Am. Chem. Soc.* **1938**, *60*, 3074.
35. P. Vanýsek, *CRC Handb. Chem. Phys.* **1996**, *96*, 5.
36. M. J. Pikal, D. G. Miller, *J. Chem. Eng. Data* **1971**, *16*, 226.
37. M. S. Moats, J. B. Hiskey, D. W. Collins, *Hydrometallurgy* **2000**, *56*, 255.
38. P. Quaino, F. Juarez, E. Santos, W. Schmickler, *Beilstein J. Nanotechnol.* **2014**, *5*, 846.
39. M. Schalenbach, F. D. Speck, M. Ledendecker, O. Kasian, D. Goehl, A. M. Mingers, B. Breitbach, H. Springer, S. Cherevko, K. J. J. Mayrhofer, *Electrochim. Acta* **2017**, *259*, 1154.
40. J. Zheng, Y. Yan, B. Xu, *J. Electrochem. Soc.* **2015**, *162*, F1470.
41. M. B. Vukmirovic, N. Vasiljevic, N. Dimitrov, K. Sieradzki, *J. Electrochem. Soc.* **2003**, *150*, B10.
42. T. Suzuki, K. Kudo, Y. Morimoto, *J. Power Sources* **2013**, *222*, 379.
43. M. Schalenbach, G. Tjarks, M. Carmo, W. Lueke, M. Mueller, D. Stolten, *J. Electrochem. Soc.* **2016**, *163*, F3197.
44. K.-D. Kreuer, *Chem. Mater.* **2014**, *26*, 361.
45. M. Schalenbach, W. Lueke, W. Lehnert, D. Stolten, *Electrochim. Acta* **2016**, *214*, 362.
46. T. Norby, *Solid State Ionics* **1999**, *125*, 1.
47. A. Weber, E. Ivers-Tiffée, *J. Power Sources* **2004**, *127*, 273.

SUPPORTING INFORMATION

Additional supporting information may be found in the online version of the article at the publisher's website.

How to cite this article: M. Schalenbach, B. Hecker, B. Schmid, Y. E. Durmus, H. Tempel, H. Kungl, R.-A. Eichel, *Electrochem. Sci. Adv*. **2023**, *3*, e2100189. https://doi.org/10.1002/elsa.202100189